

Kitaev chain in synthetic dimension with cavity-controlled Majorana modes

Adel Ali and Alexey Belyanin

Department of Physics and Astronomy, Texas A&M University, College Station, TX, 77843 USA

(Dated: May 7, 2026)

We introduce a tunable synthetic-dimension platform for realizing Kitaev-chain physics with high degree of control over Majorana zero modes. It is based on a generic Landau-quantized two dimensional electron system coupled to the magnetic flux of a superconducting LC circuit. The structured vector potential of a superconducting LC inductor induces attractive interactions between electron angular-momentum states at the lowest Landau level. These states serve as a synthetic dimension for the coveted fermionic Kitaev chain, with Majorana zero modes existing at the boundaries of the angular-momentum lattice. The crucial advantage of this proposal is the possibility of a robust, nonlocal readout and control of the Majorana states by a LC resonator. The platform relies on mature circuit QED and semiconductor technologies and provides a promising pathway to topological quantum computing.

I. INTRODUCTION

The search for controllable Majorana zero modes has become a central theme in the study of topological quantum matter. The minimal theoretical paradigm is Kitaev’s spinless p -wave chain, in which a one-dimensional superconductor enters a class-D topological phase supporting exponentially localized Majorana boundary modes [1]. More broadly, Majorana zero modes are attractive for quantum information because the fermion parity stored by spatially separated Majoranas is intrinsically nonlocal, and braiding or measurement-only protocols can implement fault-tolerant operations protected against local perturbations [2–4].

Physical realizations of Kitaev-chain physics have been pursued in several platforms. The most developed route uses semiconductor nanowires with strong spin-orbit coupling, Zeeman splitting, and proximity-induced s -wave superconductivity, which together emulate an effective spinless p -wave superconductor [5, 6]. Related proposals use topological-insulator surfaces or Josephson structures to obtain Majorana modes from conventional superconductors through spin-momentum locking and proximity pairing [7]. These platforms have led to extensive experimental progress, including zero-bias anomalies and hybrid nanowire devices suggestive of Majorana physics [8]. Nevertheless, unambiguous realization and manipulation remain challenging. The required conditions combine a hard induced superconducting gap, controlled chemical potential, sufficiently large spin-orbit coupling, strong but not destructive magnetic fields, low disorder, suppressed quasiparticle poisoning, and reliable nonlocal readout of the Majorana pair. Moreover, braiding in one-dimensional wire implementations requires networks, T-junctions, or measurement protocols rather than a single isolated chain [4, 9]. More recently, artificial Kitaev chains based on quantum-dot superconductor arrays have realized minimal two- and three-site versions of the model, highlighting both the scalability challenge of real-space implementations [10, 11]. These challenges motivate alternative routes in which the ingredients of the Kitaev chain are not provided by real-space hopping

and proximity pairing alone, but are instead engineered in a more programmable Hilbert space.

Synthetic dimensions provide precisely such a route. In a synthetic dimension, a discrete set of internal, modal, frequency, orbital, or momentum states is reinterpreted as the sites of an artificial lattice [12–14]. Couplings between these states play the role of hopping matrix elements, while phases of the couplings generate synthetic gauge fields. This idea has enabled topological lattice models in systems whose physical dimension is lower than the effective dimension of the Hamiltonian. Momentum-space lattices in cold atoms provide a particularly relevant precedent [15, 16]. Photonic frequency and orbital-angular-momentum modes provide another important setting in which modal indices are used as synthetic coordinates [17]. These developments demonstrate that a synthetic lattice need not correspond to a physical array of sites; it may instead be encoded in a controllable basis of quantum states.

In parallel, a broader research area of “cavity quantum materials” has emerged, where the electromagnetic environment is an active mediator capable of reshaping many-body interactions [18]. In particular, it has been shown that structured cavity vacuum fluctuations can mediate effective electron-electron interactions and induce superconducting pairing, including pairing channels generated by current-current interactions in two-dimensional electronic systems [19, 20]. Circuit-QED architectures provide a potentially more programmable setting for this idea: the mode profile, impedance, frequency, and inductive participation of a superconducting LC resonator can be engineered, allowing the effective interaction kernel to be shaped by circuit geometry rather than inherited from a fixed optical cavity mode [21–23].

Here we bring these developments together to propose a new synthetic route to the coveted fermionic Kitaev chain and associated Majorana physics, based on a conceptually simple system: a generic Landau-quantized two dimensional electron gas (2DEG), such as a semiconductor quantum well or graphene, coupled to a superconducting LC circuit. Other than the underlying mature technologies, its crucial advantage is naturally long

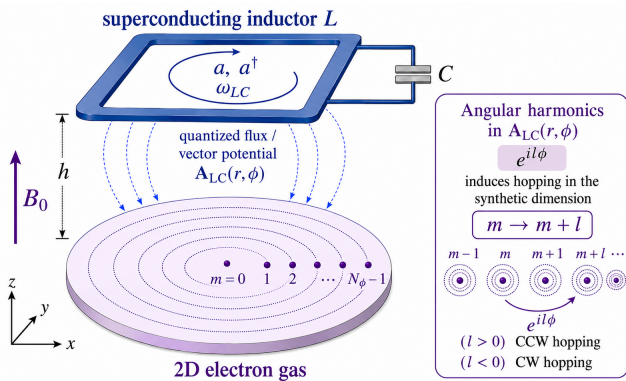


FIG. 1. Schematic of a disk-shaped 2DEG sample placed in a strong static transverse magnetic field $\mathbf{B}_0 = B_0 \hat{\mathbf{z}}$ and proximally coupled to the inductive element of a superconducting LC circuit. Angular harmonics of the circuit field, $\mathbf{A}_{\text{LC}}(r, \phi) \sim e^{i\ell\phi}$, obey the selection rule $\Delta m = \ell$, thereby inducing hopping $m \rightarrow m + \ell$ along the synthetic angular-momentum dimension. A loop geometry dominated by $\ell = 0$ and $\ell = 1$ harmonics produces the nearest-neighbor synthetic hopping needed for a Kitaev-chain-like reduction, while higher harmonics generate longer-range corrections.

chains and the possibility of a robust, nonlocal microwave readout and control of the Majorana states.

A simple conceptual example is sketched in Fig. 1. Electrons in a 2DEG sample are at the lowest Landau level (LLL) in a strong perpendicular magnetic field and coupled to a quantized vector potential supported by an LC loop, which is fabricated on a dielectric spacer of nm-scale thickness h (e.g., a quantum well barrier, or an hBN layer in the case of graphene).

In the symmetric gauge, the LLL orbitals are labeled by the guiding-center angular momentum $m = 0, 1, \dots, N_\phi - 1$, with orbital radius $R_m \simeq \sqrt{2m} \ell_B$. The index m therefore forms a natural one-dimensional synthetic coordinate with open boundaries. Although we use symmetric-gauge orbitals to represent the LLL states, the synthetic coordinate is not a gauge artifact. The physical system is a finite-size 2DEG sample with a geometry set by the lateral boundaries (or lateral confinement potential) and by the LC loop geometry. For a disk-shaped sample with a specified center, the LLL guiding-center angular momentum labels the radial position of the orbitals. [24]

Unlike cold-atom momentum-space lattices, where hopping is generated by optical momentum transfer, here hopping in the synthetic m -direction is generated by angular harmonics of a quantized magnetostatic vector potential. The coupling is purely dispersive as we assume that the LC frequency is much higher than the energies of electron m -states, so that the quantized superconducting flux mode remains in the vacuum ground state. Moreover, the same LC mode that engineers the synthetic hopping and interaction may also provide a dispersive readout channel. Therefore, flux-engineered Landau-

level synthetic dimensions offer a new route to programmable topological superconductivity beyond real-space nanowire architectures.

II. DESCRIPTION OF THE PLATFORM

We consider a spin-polarized two-dimensional electron gas in a strong classical perpendicular magnetic field $B_0 \hat{\mathbf{z}}$, coupled to a single superconducting LC mode; see Fig. 1. The classical bias vector potential and the quantized LC vector potential must enter the minimal-coupling Hamiltonian before projection onto a Landau level. For electrons of charge $-e$ and mass m^* , the total vector potential is written

$$\mathbf{A}_{\text{tot}}(\mathbf{r}) = \mathbf{A}_B(\mathbf{r}) + \hat{X} \mathbf{A}_{\text{LC}}(\mathbf{r}), \quad \hat{X} = \hat{a} + \hat{a}^\dagger, \quad (1)$$

where $\mathbf{A}_B = (B_0 r/2) \hat{\phi}$ in symmetric gauge. The continuum Hamiltonian is

$$\hat{H} = \int d^2r \hat{\psi}^\dagger(\mathbf{r}) \left[\frac{1}{2m^*} \left(-i\hbar\nabla + e\mathbf{A}_B + e\hat{X}\mathbf{A}_{\text{LC}} \right)^2 \right. \\ \left. + V_{\text{conf}}(\mathbf{r}) - \mu \right] \hat{\psi}(\mathbf{r}) + \hbar\omega_{\text{LC}} \hat{a}^\dagger \hat{a}. \quad (2)$$

Defining the mechanical momentum in the background field,

$$\mathbf{\Pi}_B = -i\hbar\nabla + e\mathbf{A}_B, \quad (4)$$

and expanding Eq. (3) in powers of \hat{X} , one obtains

$$\hat{H} = \hat{H}_B + \hbar\omega_{\text{LC}} \hat{a}^\dagger \hat{a} + \hat{X} \hat{\Gamma} + \hat{X}^2 \hat{D}, \quad (5)$$

with

$$\hat{H}_B = \int d^2r \hat{\psi}^\dagger \left[\frac{\mathbf{\Pi}_B^2}{2m^*} + V_{\text{conf}} - \mu \right] \hat{\psi}, \quad (6)$$

where

$$\hat{\Gamma} = \frac{e}{2m^*} \int d^2r \hat{\psi}^\dagger(\mathbf{r}) \{ \mathbf{A}_{\text{LC}}(\mathbf{r}), \mathbf{\Pi}_B \} \hat{\psi}(\mathbf{r}), \quad (7)$$

and

$$\hat{D} = \frac{e^2}{2m^*} \int d^2r \hat{n}(\mathbf{r}) |\mathbf{A}_{\text{LC}}(\mathbf{r})|^2. \quad (8)$$

Equation (7) is the gauge-consistent linear LC vertex. It contains both the canonical paramagnetic-current term and the cross term between the bias field B_0 and the LC vector potential. The diamagnetic term D given by Eq. (8) is retained because it is required by minimal coupling and controls the stability of the dispersive reduction.

A. Landau-level projection

We now project onto the lowest Landau. In the symmetric gauge the single-particle orbitals are

$$\phi_m(r, \phi) = \frac{1}{\sqrt{2\pi\ell_B^2 m!}} \left(\frac{r}{\sqrt{2}\ell_B}\right)^m e^{im\phi} e^{-r^2/4\ell_B^2}, \quad (9)$$

where $\ell_B = \sqrt{\hbar/eB_0}$. The projected field operator is

$$\hat{\psi}(\mathbf{r}) = \sum_{m=0}^{N_\phi-1} \phi_m(\mathbf{r}) c_m.$$

The LLL index m is therefore a one-dimensional synthetic coordinate. The projected Hamiltonian has the form

$$\hat{H}_{\text{LLL}} = \hat{H}_{\text{el}} + \hbar\omega_{\text{LC}} \hat{a}^\dagger \hat{a} + \hat{X} \hat{\Gamma}_{\text{LLL}} + \hat{X}^2 \hat{D}_{\text{LLL}}, \quad (10)$$

where

$$\hat{H}_{\text{el}} = \sum_{m,n} h_{mn}^{(0)} c_m^\dagger c_n$$

contains the confinement, disorder, and possible weak Landau-level nonflatness.

The angular structure of the LC loop controls the range of hopping in the synthetic m -direction. We take the dominant LC vector potential in the plane to be azimuthal,

$$\mathbf{A}_{\text{LC}}(r, \phi) = A_\phi(r) f(\phi) \hat{\phi}.$$

Expanding

$$f(\phi) = \sum_{\ell=-\infty}^{\infty} f_\ell e^{i\ell\phi}, \quad f_{-\ell} = f_\ell^*,$$

the LLL angular integral gives the selection rule

$$e^{i\ell\phi} \Rightarrow \Delta m = \ell.$$

For example, an $\ell = 1$ harmonic generates nearest-neighbor matrix elements $m \leftrightarrow m+1$ in the Landau-level synthetic chain.

Therefore, the geometry of the superconducting circuit directly controls the range and phase of hopping in the Landau-level synthetic dimension. In particular, a nearly circular loop with a controlled dipolar asymmetry contains dominant $\ell = 0$ and $\ell = 1$ harmonics, producing the ingredients closest to a nearest-neighbor Kitaev chain. The angular profile that best realizes the synthetic chain is

$$f(\phi) \simeq f_0 + f_1 \cos(\phi - \phi_0), \quad |f_{\ell \geq 2}| \ll |f_1| \ll |f_0|.$$

One of the geometries closest to this angular profile is a slightly off-center or single-lobed loop. Keeping only these two harmonics, the projected LC vertex is

$$\hat{\Gamma}_{\text{LLL}} = \hat{\Gamma}_0 + \hat{\Gamma}_1,$$

with

$$\hat{\Gamma}_0 = \sum_m \eta_m c_m^\dagger c_m,$$

and

$$\hat{\Gamma}_1 = \sum_m \left(\gamma_m e^{-i\phi_0} c_{m+1}^\dagger c_m + \gamma_m^* e^{i\phi_0} c_m^\dagger c_{m+1} \right).$$

The coefficients η_m and γ_m are radial LLL matrix elements determined by $A_\phi(r)$, the bias field, and the loop geometry. In the bulk of a large droplet one may approximate

$$\eta_m \simeq \eta_0, \quad \gamma_m \simeq \gamma_1,$$

up to smooth edge corrections.

B. Dispersive elimination of the LC mode.

In the off-resonant regime, the LC oscillator may be eliminated. Replacing \hat{D}_{LLL} by its expectation value $D^{(0)}$, one obtains

$$\hat{H}_{\text{eff}} = \hat{H}_{\text{el}} - g_{\text{LC}} \hat{\Gamma}_{\text{LLL}}^2, \quad g_{\text{LC}} = \frac{1}{\hbar\omega_{\text{LC}} + 4D^{(0)}}. \quad (11)$$

This form is the static limit of a Schrieffer-Wolff or oscillator completion-of-the-square reduction. Corrections are controlled by the ratios of electronic energy scales to $\hbar\omega_{\text{LC}}$.

We now show how Eq. (11) produces the Kitaev chain. In a fixed-particle-number sector, the nearly uniform $\ell = 0$ piece acts as

$$\hat{\Gamma}_0 \simeq \eta_0 N_e.$$

The cross term between $\hat{\Gamma}_0$ and $\hat{\Gamma}_1$ gives

$$-g_{\text{LC}} \left(\hat{\Gamma}_0 \hat{\Gamma}_1 + \hat{\Gamma}_1 \hat{\Gamma}_0 \right) = -t_1 \sum_m \left(e^{-i\phi_0} c_{m+1}^\dagger c_m + e^{i\phi_0} c_m^\dagger c_{m+1} \right), \quad (12)$$

where

$$t_1 = 2g_{\text{LC}} \eta_0 \gamma_1 N_e. \quad (13)$$

The phase ϕ_0 is a Peierls phase in the synthetic chain and may be removed by $c_m \rightarrow e^{im\phi_0} c_m$ for an open chain. Hence the $(\ell = 0) \times (\ell = 1)$ cross term supplies the crucial nearest-neighbor normal hopping required for a Kitaev chain.

The square of the $\ell = 1$ vertex produces subleading corrections. For uniform $\gamma_m = \gamma_1$, define

$$T_1 = \sum_m \left(c_{m+1}^\dagger c_m + c_m^\dagger c_{m+1} \right).$$

Then

$$T_1^2|_{\text{one-body}} = 2 \sum_m n_m + \sum_m \left(c_{m+2}^\dagger c_m + \text{h.c.} \right).$$

Thus Eq. (11) also generates a chemical-potential shift and a second-neighbor synthetic hopping,

$$-t_2 \sum_m \left(c_{m+2}^\dagger c_m + \text{h.c.} \right), \quad t_2 \simeq g_{\text{LC}} |\gamma_1|^2. \quad (14)$$

The desired Kitaev limit is obtained when

$$|t_2| \ll |t_1|,$$

which is naturally favored by a dominant $\ell = 0$ component and a weak dipolar distortion.

C. Reduction to Kitaev Hamiltonian

The same interaction in Eq. (11) contains a genuine two-body term. For a general one-body vertex

$$\hat{\Gamma}_{\text{LLL}} = \sum_{m,n} \Gamma_{mn} c_m^\dagger c_n,$$

normal ordering gives

$$\hat{\Gamma}_{\text{LLL}}^2 = \sum_{m,q} (\Gamma^2)_{mq} c_m^\dagger c_q - \sum_{m,n,p,q} \Gamma_{mn} \Gamma_{pq} c_m^\dagger c_p^\dagger c_n c_q.$$

Therefore

$$\hat{H}_{2b} = g_{\text{LC}} \sum_{m,n,p,q} \Gamma_{mn} \Gamma_{pq} c_m^\dagger c_p^\dagger c_n c_q. \quad (15)$$

The leading superconducting instability is obtained by solving the antisymmetrized Cooper-channel eigenvalue problem associated with Eq. (15). If the leading attractive eigenmode is the nearest-neighbor odd channel, the natural order parameter is

$$\Delta_m = U_{\text{eff}} \langle c_m c_{m+1} \rangle, \quad \Delta_m \simeq \Delta, \quad (16)$$

where $U_{\text{eff}} > 0$ denotes the magnitude of the attractive eigenvalue. This step is a controlled mean-field projection of the full interaction, not an identity: competing particle-hole orders generated by $-g_{\text{LC}} \hat{\Gamma}^2$ must be compared with the Cooper channel.

Under this Cooper-channel reduction, the mean-field pairing Hamiltonian is

$$\hat{H}_\Delta = \sum_m \left(\Delta c_m^\dagger c_{m+1}^\dagger + \Delta^* c_{m+1} c_m \right). \quad (17)$$

Combining Eqs. (12), (14), and (17) gives the extended Kitaev Hamiltonian in the angular-momentum space,

$$\begin{aligned} \hat{H}_{\text{K}}^{\text{ext}} = & -\mu_{\text{eff}} \sum_m c_m^\dagger c_m - t_1 \sum_m \left(c_{m+1}^\dagger c_m + \text{h.c.} \right) \\ & - t_2 \sum_m \left(c_{m+2}^\dagger c_m + \text{h.c.} \right) + \sum_m \left(\Delta c_m^\dagger c_{m+1}^\dagger + \text{h.c.} \right) \end{aligned} \quad (18)$$

The standard Kitaev chain is recovered in the limit $t_2/t_1 \rightarrow 0$. The open boundaries of this chain are the two ends of the Landau-level orbital sequence, $m = 0$ and $m = N_\phi - 1$.

To obtain the bulk topological criterion for the existence of Majorana edge modes, we make a Fourier transform along the synthetic dimension,

$$c_m = \frac{1}{\sqrt{N_m}} \sum_q e^{iqm} c_q.$$

Using the Nambu spinor $\Psi_q = \begin{pmatrix} c_q \\ c_{-q}^\dagger \end{pmatrix}$, one obtains

$$\hat{H}_{\text{BdG}} = \frac{1}{2} \sum_q \Psi_q^\dagger \mathcal{H}_{\text{BdG}}(q) \Psi_q,$$

with

$$\mathcal{H}_{\text{BdG}}(q) = \xi(q) \tau_z + 2|\Delta| \sin q \tau_y, \quad (19)$$

and

$$\xi(q) = -\mu_{\text{eff}} - 2t_1 \cos q - 2t_2 \cos 2q. \quad (20)$$

The quasiparticle spectrum is

$$E(q) = \sqrt{\xi^2(q) + 4|\Delta|^2 \sin^2 q}.$$

The class-D invariant changes only when the gap closes at $q = 0$ or $q = \pi$. Hence the topological criterion is

$$\xi(0)\xi(\pi) < 0, \quad (21)$$

or, explicitly,

$$(-\mu_{\text{eff}} - 2t_1 - 2t_2)(-\mu_{\text{eff}} + 2t_1 - 2t_2) < 0. \quad (22)$$

For $t_2 \ll t_1$, this reduces to the usual Kitaev condition

$$|\mu_{\text{eff}}| < 2|t_1|.$$

D. The readout scheme

A natural advantage of the proposed Landau-level synthetic Kitaev platform is that a weak LC readout mode can measure the Majorana parity dispersively. Let a_r denote the readout resonator annihilation operator, ω_r its bare frequency, and γ_i, γ_j the two Majorana zero modes whose fermion parity is

$$P_{ij} = i\gamma_i \gamma_j = \pm 1.$$

If the readout field weakly modulates a control parameter λ of the topological annulus, such as the synthetic chemical potential, hopping, pairing amplitude, or domain-wall position, then energy splitting between the two parity states ε_{ij} becomes parity dependent,

$$H_{\text{M}} = \frac{\varepsilon_{ij}(\lambda)}{2} P_{ij}.$$

Expanding $\lambda \rightarrow \lambda + \lambda_{\text{zpf}}(a_r + a_r^\dagger)$ gives a dispersive cavity shift

$$H_{\text{read}} = \hbar(\omega_r + \chi_{ij} P_{ij}) a_r^\dagger a_r, \quad \chi_{ij} \simeq \frac{\lambda_{\text{zpf}}^2}{2\hbar} \frac{\partial^2 \varepsilon_{ij}}{\partial \lambda^2}.$$

Thus the reflected microwave phase measures $P_{ij} = i\gamma_i \gamma_j$ without requiring a local tunnel probe attached to either Majorana. This is advantageous in the present system because the zero modes are synthetic-boundary modes of the angular-momentum chain, corresponding to radially separated structures in the quantum Hall droplet. Standard nanowire readout typically relies on quantum dots, tunnel contacts, Coulomb-blockaded islands, or interferometric probes near individual wire ends, whereas here the LC field naturally couples to an extended orbital operator and can provide a nonlocal, parity-sensitive, and potentially QND readout, provided $\hbar\omega_r$, the resonator linewidth $\hbar\kappa$, and $k_B T$ remain below the bulk quasiparticle gap.

III. ENERGY SCALES AND ELECTROSTATIC STABILITY

We estimate the relevant scales for a GaAs quantum well with comparable sample and LC loop radii, $R_s = R_{\text{loop}} = 4 \mu\text{m}$, $B_0 = 1 \text{ T}$, $m^* = 0.067m_e$, and $\epsilon_r = 12.9$. The magnetic length and LLL degeneracy are

$$\ell_B = 25.7 \text{ nm}, \quad N_\phi = \frac{B_0 \pi R_{\text{QH}}^2}{\Phi_0} \simeq 1.2 \times 10^4; \quad \Phi_0 = \frac{h}{e}.$$

We take the LC-loop height to be $h_{\text{LC}} = 2 \text{ nm}$, and assume the metallic (or highly doped) screening gate at a distance d below the 2DEG, typically tens of nm.

For an LC mode with $f_{\text{LC}} = 100 \text{ GHz}$ and $L = 1 \text{ pH}$,

$$\hbar\omega_{\text{LC}} = 414 \mu\text{eV}, \quad I_{\text{zpf}} = \sqrt{\frac{\hbar\omega_{\text{LC}}}{2L}} \simeq 5.8 \mu\text{A},$$

giving

$$B_{\text{zpf}} \sim \frac{\mu_0 I_{\text{zpf}}}{2R_{\text{loop}}} \simeq 0.9 \mu\text{T}, \quad \Phi_{\text{zpf}}/\Phi_0 \sim 1.1 \times 10^{-2}.$$

The corresponding edge-orbital matrix element is estimated as $\gamma_{\text{edge}} \sim 9.5 \mu\text{eV}$; see the Supplemental Material. For a strongly dipolar loop profile,

$$\epsilon_1 \equiv |\gamma_1/\gamma_0| \simeq 0.3,$$

the $\ell = 1$ matrix element is $\gamma_1 \sim 2.9 \mu\text{eV}$, and

$$V_{\text{LC}}^{(1)} \sim \frac{\gamma_1^2}{\hbar\omega_{\text{LC}}} \simeq 2.0 \times 10^{-2} \mu\text{eV}.$$

For an active Kitaev window of $N_{\text{act}} \sim 10^3$ partially filled LLL orbitals, the collective odd-channel eigenvalue is therefore

$$\lambda_{\text{LC}}^{\text{odd}} \sim N_{\text{act}} V_{\text{LC}}^{(1)} \sim 20 \mu\text{eV}.$$

We thus estimate an induced pairing scale $\Delta_1 \sim 10 - 20 \mu\text{eV}$, and hence a topological gap

$$E_{\text{gap}} = \min_q \sqrt{\xi^2(q) + 4|\Delta_1|^2 \sin^2 q} \simeq 2|\Delta_1| \sim 20-40 \mu\text{eV},$$

corresponding to

$$T_{\text{gap}} \sim 0.2 - 0.5 \text{ K}.$$

The relevant electrostatic energy is the LLL-projected adjacent-bond cost in the same pairing channel,

$$U_m^C = \langle m, m+1 | V_C | m, m+1 \rangle_A,$$

not the full Coulomb energy. A metallic gate at distance d gives the screened interaction

$$V_C(q) = \frac{e^2}{2\epsilon_0 \epsilon_r q} (1 - e^{-2qd}).$$

Taking $d = 30 \text{ nm}$ as an example, the central value is large,

$$U_0^C \simeq 0.67 \text{ meV},$$

so the pairing near $m = 0$ is strongly suppressed. However, the adjacent-bond cost falls rapidly at large angular momenta because the orbitals become extended annuli. In an annulus with $R_{\text{in}} = 2 \mu\text{m}$, $R_{\text{out}} = 4 \mu\text{m}$, the active m -window is

$$m_{\text{in/out}} \simeq \frac{R_{\text{in/out}}^2}{2\ell_B^2}, \quad \text{or } m_{\text{in}} \simeq 3.0 \times 10^3, \quad m_{\text{out}} \simeq 1.2 \times 10^4.$$

Within this window, the screened adjacent-bond repulsion is only

$$U_{m_{\text{in}}}^C \sim 2 \times 10^{-2} \mu\text{eV}, \quad U_{m_{\text{out}}}^C \sim 3 \times 10^{-3} \mu\text{eV},$$

which is negligible compared with the estimated gap $E_{\text{gap}} \sim 20 - 40 \mu\text{eV}$. Thus a gate-screened or annular geometry as in Fig. 2(d) removes the small- m orbitals where electrostatic repulsion is largest and places the active synthetic Kitaev chain in a regime where Coulomb repulsion does not destroy the pairing instability.

Finally, the dispersive condition is controlled by

$$E_{\text{gap}}/\hbar\omega_{\text{LC}} \sim 0.05 - 0.10.$$

At $B_0 = 1 \text{ T}$, the GaAs cyclotron energy is

$$\hbar\omega_c = \frac{\hbar e B_0}{m^*} \simeq 1.73 \text{ meV},$$

so the 100 GHz LC mode remains below the inter-Landau-level cyclotron transition. The chosen frequency is therefore high enough to justify integrating out the LC mode on the Kitaev scale, while remaining detuned from cyclotron Landau-polariton mixing.

As shown in the Supplemental Material, the estimates are even more favorable for InSb quantum wells due to about 5 times lower effective electron mass and stronger dielectric screening. In particular, one obtains about 5-10 higher topological gap and the gap temperature.

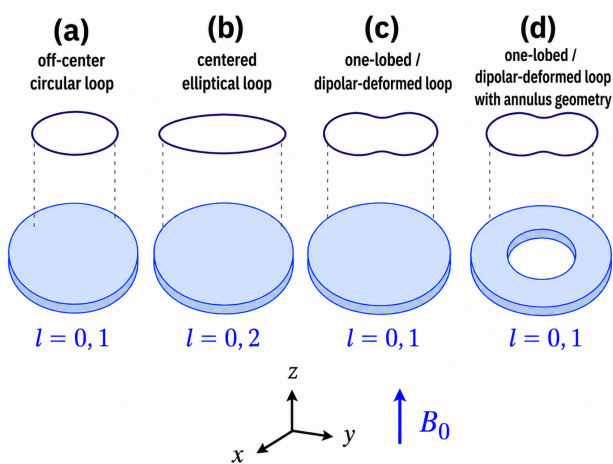


FIG. 2. Representative loop geometries for the inductive element of the superconducting LC circuit, shown above a 2DEG sample in a strong perpendicular magnetic field $B_0 \hat{z}$, with dominant angular harmonics ℓ indicated. The geometries dominated by $\ell = 0$ and $\ell = 1$ provide the closest route to a nearest-neighbor Kitaev-chain Hamiltonian, while even-harmonic geometries generate longer-range or two-sublattice couplings.

IV. GEOMETRY AND FABRICATION CONSIDERATIONS

Beyond the primary instability discussed above, the same architecture provides a direct route to engineering interactions in the synthetic orbital dimension. The LC loop defines a quantized current

$$\hat{I} = I_{\text{zpf}} (\hat{a} + \hat{a}^\dagger), \quad I_{\text{zpf}} = \sqrt{\frac{\hbar \omega_{LC}}{2L}}, \quad (23)$$

where L is the loop inductance. For a lithographically defined wire contour \mathcal{C} , the vector potential per unit current is

$$\mathbf{a}_{\mathcal{C}}(\mathbf{r}) = \frac{\mu_0}{4\pi} \oint_{\mathcal{C}} \frac{d\mathbf{R}}{|\mathbf{r} - \mathbf{R}|}. \quad (24)$$

Consequently, the paramagnetic light-matter coupling takes the compact form

$$\hat{H}_{\text{para}} = - \int d^2r \hat{\mathbf{j}}_p(\mathbf{r}) \cdot \mathbf{a}_{\mathcal{C}}(\mathbf{r}) I_{\text{zpf}} (\hat{a} + \hat{a}^\dagger) = -(\hat{a} + \hat{a}^\dagger) \hat{J}_{\mathcal{C}}.$$

This expression makes it explicit that the matter operator $\hat{J}_{\mathcal{C}}$ inherits the spatial and angular structure of the fabricated loop. Thus, by shaping \mathcal{C} , one controls the harmonic content of $\mathbf{a}_{\mathcal{C}}$ and hence the selection rules and matrix elements between different synthetic-dimension states, such as angular-momentum orbitals in a Landau-quantized 2DEG sample. The loop geometry therefore acts as a lithographically programmable interaction kernel rather than merely as a passive mode. The geometry determines which synthetic hoppings are generated, as

sketched in Fig. 2. A centered circular loop gives only an $\ell = 0$ vertex and therefore no nearest-neighbor synthetic hopping. A centered ellipse has inversion symmetry, $f(\phi + \pi) = f(\phi)$, and therefore contains mainly even harmonics,

$$f_{\text{ellipse}}(\phi) = f_0 + f_2 \cos 2\phi + f_4 \cos 4\phi + \dots$$

It naturally generates $m \rightarrow m \pm 2$ and higher even-range processes, producing two-sublattice extended Kitaev physics rather than the single-chain Kitaev limit.

The optimal geometry for the present proposal is instead a nearly circular loop with a controlled dipolar asymmetry,

$$R_{\text{loop}}(\phi) = R_0 [1 + \epsilon \cos(\phi - \phi_0)], \quad \epsilon < 1, \quad (25)$$

or equivalently a circular loop displaced slightly from the center of the electron droplet. Such a geometry produces

$$f(\phi) = f_0 + f_1 \cos(\phi - \phi_0) + O(\epsilon^2),$$

so that the unwanted higher harmonics are parametrically suppressed. The design rule for approaching the Kitaev limit is therefore

$$|f_0 f_1| \text{ large}, \quad |f_{\ell \geq 2}| \text{ small}.$$

This can be implemented using standard planar superconducting-circuit fabrication: a lithographic LC loop, SQUID loop, or high-kinetic-inductance superconducting trace can be patterned with a small displacement, a smooth single-lobed deformation, or a local side bulge. The smooth one-lobed design is preferred over sharp notches because it enhances the desired $\ell = 1$ harmonic without introducing large high- ℓ Fourier components.

V. CONCLUSIONS

We have shown a circuit-QED route to synthetic Kitaev-chain physics in a Landau-quantized two-dimensional electron system. The natural one-dimensional synthetic lattice in LLL, with the structured magnetostatic vector potential of a superconducting LC resonator generates controlled couplings and effective attractive interactions within this lattice. For suitable angular harmonics of the LC field, the resulting projected Hamiltonian maps onto an effective fermionic Kitaev chain. This provides a route to long effective chains. In addition, electrostatic confinement can tune the occupied angular-momentum window, while circuit parameters such as the resonator frequency, impedance, and inductive participation control the strength and structure of the mediated interaction. The same mode that engineers the interaction or a different weakly coupled mode offers a natural nonlocal channel for dispersive readout and control of the Majorana degrees of freedom.

These features make our proposal a promising architecture for programmable topological superconductivity. Future work will address measurement protocols, and synthetic-dimension braiding schemes based on time-dependent gates and cavity drives, including measurement-only protocols [4].

Recent theoretical and experimental developments in Quantum Hall systems coupled to cavity resonators [25–32] show that cavity vacuum fields can generate effective nonlocal electronic processes in Landau-quantized matter. These experiments share similar ingredients with our proposed platform. An important extension would be to replace the Landau level quantization by Chern-band or anomalous Quantum Hall platforms, where synthetic orbital structures could be engineered without a large applied magnetic field.

ACKNOWLEDGMENTS

This work has been supported in part by the Keck Foundation (Award No. CRM:0132347) and by the Laboratory Directed Research and Development program and Sandia University Partnerships Network (SUPN) program and performed in part at the Center for Integrated Nanotechnologies (CINT), an Office of Science User Facility operated for the U.S. Department of Energy (DOE) Office of Science. Sandia National Laboratories is a multi-mission laboratory managed and operated by National Technology and Engineering Solutions of Sandia, LLC., a wholly owned subsidiary of Honeywell International, Inc., for the U.S. Department of Energy’s National Nuclear Security Administration under Contract No. DE-NA0003525. This article describes objective technical results and analysis. Any subjective views or opinions that might be expressed in the article do not necessarily represent the views of the U.S. Department of Energy or the United States Government.

Appendix A: Estimate of LC-induced gap and Coulomb cost

We describe in more detail our estimates used in the main text. We will use the numerical values of the parameters as in the main text, namely,

$$R_{\text{QH}} = R_{\text{loop}} = 4 \mu\text{m}, \quad B_0 = 1 \text{ T}, \quad L = 1 \text{ pH}, \\ h_{\text{LC}} = 2 \text{ nm}, \quad d = 30 \text{ nm}.$$

The magnetic length and Landau-level degeneracy are

$$\ell_B = \sqrt{\frac{\hbar}{eB_0}} = 25.7 \text{ nm}, \quad N_\phi = \frac{B_0 \pi R_{\text{QH}}^2}{\Phi_0} \simeq 1.2 \times 10^4.$$

For an LC mode of frequency $f_{\text{LC}} = \omega_{\text{LC}}/2\pi$,

$$I_{\text{zpf}} = \sqrt{\frac{\hbar \omega_{\text{LC}}}{2L}}, \quad B_{\text{zpf}} \sim \frac{\mu_0 I_{\text{zpf}}}{2R_{\text{loop}}}.$$

TABLE I. Representative LC-induced scales for GaAs and InSb quantum Hall droplets. The pairing scale is quoted as an estimate because it depends on the active-window profile and the self-consistent odd-channel susceptibility.

	GaAs	InSb
f_{LC}	100 GHz	300 GHz
$\hbar \omega_{\text{LC}}$	414 μeV	1.24 meV
I_{zpf}	5.8 μA	10 μA
B_{zpf}	0.9 μT	1.6 μT
Φ_{zpf}/Φ_0	1.1×10^{-2}	1.9×10^{-2}
γ_{edge}	9.5 μeV	79 μeV
γ_1	2.9 μeV	24 μeV
$V_{\text{LC}}^{(1)}$	$2.0 \times 10^{-2} \mu\text{eV}$	0.45 μeV
$\lambda_{\text{LC}}^{\text{odd}}$	20 μeV	0.45 meV
Δ_1	10 – 20 μeV	0.2 – 0.45 meV
E_{gap}	20 – 40 μeV	0.45 – 0.9 meV
T_{gap}	0.2 – 0.5 K	5 – 10 K
$E_{\text{gap}}/\hbar \omega_{\text{LC}}$	0.05 – 0.10	0.36 – 0.72

The corresponding zero-point flux through the 2DEG sample is

$$\frac{\Phi_{\text{zpf}}}{\Phi_0} \sim \frac{B_{\text{zpf}} \pi R_{\text{QH}}^2}{\Phi_0}.$$

A crude estimate of the orbital matrix element at the edge of the sample is obtained from the paramagnetic vertex,

$$\gamma_{\text{edge}} \sim \frac{e}{m^*} A_{\text{zpf}}(R) p_{B,\phi}(R) \sim \frac{e^2 B_0 B_{\text{zpf}} R_{\text{QH}}^2}{4m^*},$$

where $A_{\text{zpf}}(R) \sim B_{\text{zpf}} R/2$ and $p_{B,\phi}(R) \sim eB_0 R/2$. For a loop profile with the first harmonic weight $\epsilon_1 = |\gamma_1/\gamma_0| \simeq 0.3$,

$$\gamma_1 \simeq \epsilon_1 \gamma_{\text{edge}}, \quad V_{\text{LC}}^{(1)} \sim \frac{\gamma_1^2}{\hbar \omega_{\text{LC}}}, \quad \lambda_{\text{LC}}^{\text{odd}} \sim N_{\text{act}} V_{\text{LC}}^{(1)},$$

with $N_{\text{act}} \sim 10^3$ active LLL orbitals. The resulting synthetic Kitaev gap is estimated from

$$E_{\text{gap}} = \min_q \sqrt{\xi^2(q) + 4|\Delta_1|^2 \sin^2 q},$$

where $\xi(q) = -\mu_{\text{eff}} - 2t_1 \cos q - 2t_2 \cos 2q$.

Near $\mu_{\text{eff}} \simeq 0$ and for $|t_2| \ll |t_1|$,

$$E_{\text{gap}} \simeq 2|\Delta_1|.$$

The numerical estimates are collected in Table I. The GaAs values use $m^* = 0.067m_e$, $\epsilon_r = 12.9$, and $f_{\text{LC}} = 100 \text{ GHz}$; the InSb values are obtained using the same geometry but with $m^* = 0.014m_e$, $\epsilon_r = 16.8$, and $f_{\text{LC}} = 300 \text{ GHz}$.

We next estimate the screened Coulomb cost in the same adjacent-orbital pairing channel. For a metallic screening plane at distance d ,

$$V_C(q) = \frac{e^2}{2\epsilon_0\epsilon_r q} (1 - e^{-2qd}).$$

The LLL pseudopotentials are

$$V_\ell^C(d) = \frac{e^2}{4\pi\epsilon_0\epsilon_r\ell_B} \int_0^\infty dx (1 - e^{-2dx/\ell_B}) L_\ell(x^2) e^{-x^2}.$$

The antisymmetrized adjacent-orbital cost is

$$U_m^C(d) = \langle m, m+1 | V_C | m, m+1 \rangle_A = \sum_{k=0}^m w_{m,k} V_{2k+1}^C(d),$$

with

$$w_{m,k} = \frac{\binom{m}{k}^2 (2m-2k)! (2k+1)!}{4^m m! (m+1)!}.$$

For $m=0$, $U_0^C = V_1^C$, which yields

$$U_0^C \simeq 0.67 \text{ meV (GaAs)}, \quad U_0^C \simeq 0.51 \text{ meV (InSb)}.$$

Thus, pairing near the origin $R=0$ is electrostatically unfavorable. This constraint is removed in an annulus of a finite radius. For

$$R_{\text{in}} = 2 \mu\text{m}, \quad R_{\text{out}} = 4 \mu\text{m},$$

the active orbital window is

$$m_{\text{in/out}} \simeq \frac{R_{\text{in/out}}^2}{2\ell_B^2}, \quad m_{\text{in}} \simeq 3.0 \times 10^3, \quad m_{\text{out}} \simeq 1.2 \times 10^4.$$

In this large- m window the screened adjacent-bond repulsion is strongly suppressed:

$$\begin{aligned} \text{GaAs: } U_{m_{\text{in}}}^C &\sim 2 \times 10^{-2} \mu\text{eV}, \quad U_{m_{\text{out}}}^C \sim 3 \times 10^{-3} \mu\text{eV}, \\ \text{InSb: } U_{m_{\text{in}}}^C &\sim 1.5 \times 10^{-2} \mu\text{eV}, \quad U_{m_{\text{out}}}^C \sim 2.3 \times 10^{-3} \mu\text{eV}. \end{aligned}$$

These values are negligible compared with the estimated LC-induced gaps in Table I. The annular geometry therefore removes the small- m orbitals where Coulomb repulsion is largest and places the synthetic Kitaev chain in a large-radius window where screened electrostatic repulsion does not compete with the induced odd-channel pairing.

Finally, the relevant single-particle gaps remain favorable. At $B_0 = 1 \text{ T}$,

$$\hbar\omega_c = \frac{\hbar e B_0}{m^*} \simeq 1.73 \text{ meV (GaAs)}, \quad 8.3 \text{ meV (InSb)}.$$

Thus the LC mode lies below the inter-Landau-level transition in both materials. In InSb, the Zeeman scale is also large:

$$E_Z = |g^*| \mu_B B_0 \simeq 2.0 \text{ meV} \quad (|g^*| \simeq 35),$$

supporting a spin-polarized description. The main constraint in the InSb case is instead a marginal dispersive hierarchy, $E_{\text{gap}}/\hbar\omega_{\text{LC}} \sim 0.36 - 0.72$; a conservative regime therefore uses the lower part of the estimated gap range or a smaller active window N_{act} .

-
- [1] A. Y. Kitaev, *Physics-Uspekhi* **44**, 131 (2001).
[2] C. Nayak, S. H. Simon, A. Stern, M. Freedman, and S. Das Sarma, *Reviews of Modern Physics* **80**, 1083 (2008), arXiv:0707.1889.
[3] J. Alicea, *Reports on Progress in Physics* **75**, 076501 (2012), arXiv:1202.1293.
[4] D. Aasen, M. Hell, R. V. Mishmash, A. Higginbotham, J. Danon, M. Leijnse, T. S. Jespersen, J. A. Folk, C. M. Marcus, K. Flensberg, and J. Alicea, *Physical Review X* **6**, 031016 (2016), arXiv:1511.05153.
[5] R. M. Lutchyn, J. D. Sau, and S. Das Sarma, *Physical Review Letters* **105**, 077001 (2010), arXiv:1002.4033.
[6] Y. Oreg, G. Refael, and F. von Oppen, *Physical Review Letters* **105**, 177002 (2010), arXiv:1003.1145.
[7] L. Fu and C. L. Kane, *Physical Review Letters* **100**, 096407 (2008), arXiv:0707.1692.
[8] V. Mourik, K. Zuo, S. M. Frolov, S. R. Plissard, E. P. A. M. Bakkers, and L. P. Kouwenhoven, *Science* **336**, 1003 (2012), arXiv:1204.2792.
[9] J. Alicea, Y. Oreg, G. Refael, F. von Oppen, and M. P. A. Fisher, *Nature Physics* **7**, 412 (2011), arXiv:1006.4395.
[10] T. Dvir, G. Wang, N. van Loo, C.-X. Liu, G. P. Mazur, A. Bordin, S. L. D. ten Haaf, J.-Y. Wang, D. van Driel, F. Zatelli, X. Li, F. K. Malinowski, S. Gazibegovic, G. Badawy, E. P. A. M. Bakkers, M. Wimmer, and L. P. Kouwenhoven, *Nature* **614**, 445 (2023).
[11] A. Bordin, C.-X. Liu, T. Dvir, F. Zatelli, S. L. D. ten Haaf, D. van Driel, G. Wang, N. van Loo, Y. Zhang, J. C. Wolff, T. Van Caekenberghe, M. Wimmer, L. P. Kouwenhoven, and G. P. Mazur, *Nature Nanotechnology* **20**, 726 (2025).
[12] O. Boada, A. Celi, J. I. Latorre, and M. Lewenstein, *Physical Review Letters* **108**, 133001 (2012), arXiv:1112.1019.
[13] A. Celi, P. Massignan, J. Ruseckas, N. Goldman, I. B. Spielman, G. Juzeliunas, and M. Lewenstein, *Physical Review Letters* **112**, 043001 (2014), arXiv:1307.8349.
[14] T. Ozawa and H. M. Price, *Nature Reviews Physics* **1**, 349 (2019).
[15] E. J. Meier, F. A. An, and B. Gadway, *Nature Communications* **7**, 13986 (2016), arXiv:1607.02811.
[16] F. A. An, E. J. Meier, J. Ang'ong'a, and B. Gadway, *Physical Review Letters* **120**, 040407 (2018).
[17] L. Yuan, Q. Lin, M. Xiao, and S. Fan, *Optica* **5**, 1396

- (2018).
- [18] F. Schlawin, D. M. Kennes, and M. A. Sentef, *Applied Physics Reviews* **9**, 011312 (2022), arXiv:2112.15018.
- [19] F. Schlawin, A. Cavalleri, and D. Jaksch, *Physical Review Letters* **122**, 133602 (2019), arXiv:1804.07142.
- [20] A. Chakraborty, F. Piazza, and E. Sela, *Physical Review Letters* **127**, 177002 (2021).
- [21] A. Blais, A. L. Grimsmo, S. M. Girvin, and A. Wallraff, *Reviews of Modern Physics* **93**, 025005 (2021), arXiv:2005.12667.
- [22] P. Krantz, M. Kjaergaard, F. Yan, T. P. Orlando, S. Gustavsson, and W. D. Oliver, *Applied Physics Reviews* **6**, 021318 (2019), arXiv:1904.06560.
- [23] A. Ali and A. Belyanin, (2026), arXiv:2604.12544 [cond-mat.mes-hall].
- [24] A different gauge would represent the same projected operators in a different basis, but it would not change the spectrum or the existence of topological domain walls. The compact nearest-neighbor form of the synthetic chain is therefore a consequence of the rotational structure of the physical sample and circuit field, not of an arbitrary gauge choice.
- [25] D. Hagenmüller, S. De Liberato, and C. Ciuti, *Physical Review B* **81**, 235303 (2010).
- [26] G. Scalari, C. Maissen, D. Turčinková, D. Hagenmüller, S. De Liberato, C. Ciuti, D. Schuh, C. Reichl, W. Wegscheider, M. Beck, and J. Faist, *Science* **335**, 1323 (2012).
- [27] C. Maissen, G. Scalari, F. Valmorra, M. Beck, J. Faist, S. Cibella, R. Leoni, C. Reichl, C. Charpentier, and W. Wegscheider, *Physical Review B* **90**, 205309 (2014).
- [28] F. Appugliese, J. Enkner, G. L. Paravicini-Bagliani, M. Beck, C. Reichl, W. Wegscheider, G. Scalari, C. Ciuti, and J. Faist, *Science* **375**, 1030 (2022).
- [29] J. Enkner, L. Graziotto, F. Appugliese, V. Rokaj, J. Wang, M. Ruggenthaler, C. Reichl, W. Wegscheider, A. Rubio, and J. Faist, *Physical Review X* **14**, 021038 (2024).
- [30] J. Enkner *et al.*, *Nature* **641**, 899 (2025).
- [31] C. Ciuti, *Physical Review B* **104**, 155307 (2021).
- [32] V. Rokaj, M. Penz, M. A. Sentef, M. Ruggenthaler, and A. Rubio, *Physical Review B* **105**, 205424 (2022).